This is the peer reviewed version of the following article:

Janićijević, Ž., Ninkov, M., Kataranovski, M., Radovanović, F., n.d. Poly(DL-Lactide-co-ε-Caprolactone)/Poly(Acrylic Acid) Composite Implant for Controlled Delivery of Cationic Drugs. Macromolecular Bioscience, Article No. 1800322. https://doi.org/10.1002/mabi.201800322

**Full Paper**

# Poly(DL-lactide-*co*-ε-caprolactone)/poly(acrylic acid) composite implant for controlled delivery of cationic drugs[a]

Željko Janićijević, Marina Ninkov, Milena Kataranovski, Filip Radovanović*

--------

Ž. Janićijević
University of Belgrade, School of Electrical Engineering, Bulevar kralja Aleksandra 73, 11120 Belgrade, Serbia
Ž. Janićijević, Dr. F. Radovanović
Institute of Technical Sciences of the Serbian Academy of Sciences and Arts, Knez Mihailova 35/IV, 11000 Belgrade, Serbia
E-mail: filip.radovanovic@itn.sanu.ac.rs
Dr. M. Ninkov, Prof. M. Kataranovski
Department of Ecology, Institute for Biological Research ''Siniša Stanković'', University of Belgrade, Bulevar despota Stefana 142, 11060 Belgrade, Serbia
Prof. M. Kataranovski
Department of Physiology and Biochemistry, University of Belgrade, Studenstki trg 16, 11000, Belgrade, Serbia

--------

Poly(DL-lactide-*co*-ε-caprolactone)/poly(acrylic acid) implantable composite reservoirs for cationic drugs are synthesized by sequentially applying photoirradiation and liquid phase inversion. The chemical composition and microstructure of reservoirs are characterized with FTIR-ATR and SEM, respectively. Drug loading and release properties are investigated using methylene blue as the drug model. Biocompatibility of reservoirs is examined through a series of in vitro tests and an in vivo experiment of subcutaneous implantation in Dark Agouti rats. Reservoirs show good ion-exchange capacity, high water content and fast reversible swelling with retained geometry. Results of drug loading and release reveal excellent loading efficiency and diffusion-controlled release during two weeks. Biocompatibility tests in vitro demonstrate the lack of implant proinflammatory potential and hindered adhesion of L929

--------

[a] **Supporting Information** is available online from the Wiley Online Library or from the author.

cells on the implant surface. Implants exhibit low acute toxicity and elicit a normal acute foreign body reaction that reaches the early stages of fibrous capsule formation after seven days.
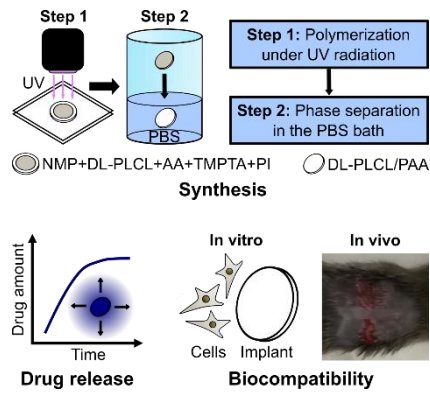
# 1. Introduction

Implantable systems are a promising approach for the delivery of drugs that cannot be efficiently delivered via the oral route or when site-specific dosing is beneficial for the patient. Prominent material classes used in drug delivery implants are biodegradable polymers and hydrogels.

Biodegradable polymers commonly found in implantable drug delivery systems are poly(lactic acid) (PLA), poly(lactic-*co*-glycolic acid) (PLGA), poly(caprolactone) (PCL), or their block copolymers.[1] These biodegradable polymers offer the advantage of avoiding surgical procedure for implant removal because they are safely metabolized and absorbed or released by excretion from the body.[2,3]

Hydrogels are cross-linked polymeric networks with high water content and physical properties resembling soft tissues of the body. Adjustable physical properties, controllable degradation, good biocompatibility, and capability for facile encapsulation of hydrophilic drugs are major advantages favoring the use of hydrogels in controlled drug release systems.[4]

Hydrogels containing functional groups with fixed charges act as polyelectrolytes in aqueous solutions. Such behavior can be exploited to control the release of charged drugs via nonspecific electrostatic interaction.[5,6] Release of these charged drugs occurs by ion exchange with mobile counter ions of the surrounding medium. Analogous to the pharmaceutical grade ion-exchange resins, charged hydrogels exhibit high drug loading capacity[7] and enhance drug stability[8]. Poly(acrylic acid) (PAA) hydrogel is an interesting material for the controlled delivery of cationic drugs because of abundant carboxyl groups enabling cation exchange.[9] Carboxyl groups on the surface of a biomaterial may have additional functions in vivo, such as the reduction of the inflammatory response and the suppression of fibrotic capsule formation which would facilitate drug release.[10]

However, pure PAA hydrogel has unfavorable mechanical properties. It exhibits a very high swelling degree under physiological conditions[11] and may suffer from spatial gel inhomogeneity[12] which is typical for hydrogels. PAA hydrogel can be reinforced with a more stable polymer matrix by forming a composite material to alleviate mechanical instability.

Composite materials comprising a biodegradable polymer and a functional PAA hydrogel could be useful as implantable reservoirs for controlled delivery of cationic drugs. Copolymerization of PAA and chitosan was used in the past to obtain biocompatible magnetic microspheres[13] and composite membranes with antibacterial properties[14]. Stankevich et al. fabricated composites of PAA and PLA for biomedical applications by immobilizing PAA as a chemically reactive cross-linker on the surface of PLA.[15]

In our previous work, we synthesized the poly(ether sulfone)/PAA composite hydrogel membrane reservoirs for transdermal delivery of cationic drug formulations by sequential application of photoirradiation and immersion precipitation.[16] As we show here, this innovative synthesis method can be modified and adapted for the fabrication of implantable drug reservoirs.

In this study, we present the synthesis and characterization of poly(DL-lactide-*co*-ε-caprolactone)/PAA implantable drug reservoir for controlled release of cationic drugs. The microstructure of the implants is imaged using Scanning electron microscopy (SEM), and their chemical composition is examined with Fourier transform infrared spectroscopy-Attenuated total reflection (FTIR-ATR). We investigate the loading capacity and in vitro release kinetics for methylene blue (MB) as a cationic model drug. Biocompatibility of the unloaded implant is tested in vitro using L929 mouse fibroblast cell line and splenocytes isolated from male Dark Agouti rat. Finally, we perform a pilot experiment for the preliminary assessment of acute in vivo response to the subcutaneously implanted unloaded drug reservoirs. Subcutaneous tissue is chosen as a representative implantation site which is

preferred for implantable drug reservoirs because it exhibits adequate hemoperfusion, low innervation, reduced risk of local inflammation, and high fat content beneficial for retarding drug absorption.[17]

## 2. Experimental Section

### 2.1. Materials

25:75 poly(DL-lactide-*co*-ε-caprolactone) (DL-PLCL) ($M_w$ = 96700, PDI = 1.61) was obtained from DURECT Corporation. N-methyl-2-pyrrolidone (NMP) (99%), acrylic acid (AA) (99%), and trimethylolpropane ethoxylate triacrylate (TMPTA) (average $M_n$ ~ 912) were supplied by Sigma-Aldrich. Photoinitiator (PI), bis(2,4,6-trimethylbenzoyl)-phenylphosphineoxide (Irgacure 819), was kindly provided by Ciba SC. MB powder (Reag. Ph Eur) was obtained from E. Merck. 3-(4,5-dimethyl-thiazol-2-yl)-2,5-diphenyltetrazolium bromide (MTT) (≥97.5%), crystal violet (≥90%), N-(1-naphthyl) ethylenediamine dihydrochloride (≥98%), and sulphanilamide (≥99%) were supplied by Sigma. Sodium hydroxide (NaOH) (p.a., >98%), phosphoric acid (ortho-Phosphoric acid, p.a., >85%), sodium chloride (NaCl) (p.a., >99.5%), potassium chloride (KCl) (p.a., >99%), di-Sodium hydrogen phosphate ($Na_2HPO_4$) (p.a., >98%), and potassium dihydrogen phosphate ($KH_2PO_4$) (p.a., >99%) were purchased from Centrohem, Stara Pazova, Serbia. Hydrochloric acid (HCl) (37%) and *n*-heptane (≥99%) were supplied by VWR Chemicals. Ethanol (p.a.) and 96 vol% ethanol were obtained from Zorka Pharma, Šabac, Serbia.

Phosphate-buffered saline (PBS) for the experiments related to implant preparation, implant swelling degree, implant swelling kinetics, MB absorption, and MB release in vitro was prepared by titration of the aqueous solution of $KH_2PO_4$ with the aqueous solution of NaOH until the pH = 7.4 and ionic strength $I$ = 0.154 M were reached. PBS used in biocompatibility tests was prepared by dissolving 8 g of NaCl, 0.2 g of KCl, 1.44 g of $Na_2HPO_4$, and 0.24 g of

KH$_2$PO$_4$ in 800 mL of distilled water. pH of the solution was adjusted to 7.4 if necessary and distilled water was finally added to obtain a total volume of 1 L.

Culture medium RPMI-1640 (Biowest, Nuaille, France) supplemented with 2 mM glutamine, 20 mg mL$^{-1}$ gentamycin (Galenika a. d., Zemun, Serbia), and 5 vol% heat-inactivated fetal calf serum (FCS) (Biowest, Nuaille, France) was used for in vitro and in vivo tests. For use in experiments, Concanavalin A (ConA) from Canavalia ensiformis (Jack bean), Type IV-S (Sigma Chemical Co., St. Louis, MO, USA) was dissolved in RPMI-1640 medium. MTT and crystal violet were dissolved in PBS. Griess reagent was prepared by mixing equal volumes of 0.1% N-(1-naphthyl) ethylenediamine dihydrochloride dissolved in water and 1% sulphanilamide in 5% phosphoric acid solution in water.

All chemicals were used as received without further purification. Distilled water was used to prepare all aqueous solutions in our experiments. All solutions for cell culture experiments were prepared under sterile conditions and were sterile filtered (Minisart, pore size 0.20 μm, Sartorius Stedim Biotech, Goettingen, Germany) before use.

Teflon rings (PTFE Flat Washer) had the nominal thickness of 0.787 mm and a hole size of 11.11 mm. Fluorinated ethylene propylene non-stick film of 25 μm thickness was supplied by Scientific Commodities, Inc.. Flasks and plates for cell cultivation were purchased from Nunc (Hannover, Germany).

## 2.2. Implant preparation

For the preparation of composite implants, the traditional liquid phase inversion process for making membranes[18] was modified by incorporating AA and a trifunctional cross-linker (TMPTA) in the polymer solution and copolymerizing them before the immersion in the PBS. A 30 wt% solution of DL-PLCL in NMP was prepared by mixing overnight. Solutions of AA, TMPTA, and PI in NMP were freshly prepared by mixing the components in amber vials cooled with ice and protected from ambient light. The solution for making implants was prepared by mixing a given quantity of DL-PLCL solution with a solution of

photopolymerizable components just prior to the experiment. All prepared solutions were transparent confirming complete miscibility of the components. DL-PLCL concentration in the solution is expressed in wt%. AA concentration is expressed in mmol $g^{-1}$ of the final dry implant at a theoretical 100% reactant conversion. The concentration of the cross-linking agent is expressed as a mol% based on the AA concentration.

The prepared solution was dispensed into a non-stick mold constructed by sealing the Teflon ring at the top and bottom with layers of transparent non-stick film to prevent leakage and oxygen penetration. The solution was subsequently exposed to UV irradiation of the wavelength $\lambda = 365$ nm through a glass plate on top of the mold for 3 min. The exposure dose measured by the YK-35UV light meter was 3.6 J $cm^{-2}$. Polymerization and cross-linking of AA were initiated by UV exposure to create a gel in the starting solution. After UV curing, a non-stick plunger was used to drop the gel into the PBS bath to form a disk-shaped implant. Implants were left in the PBS bath overnight to complete phase separation and solidification, and to extract residual unreacted components. Implants were then immersed in the fresh PBS solution and kept refrigerated to prevent microbial contamination and retard the degradation process. Implants intended for in vitro and in vivo biocompatibility tests were prepared in a laminar flow hood under sterile conditions. These implants were left in the sterile filtered buffer for 24 h at 4 °C to extract the remaining solvent, unreacted monomers, and PI. Implants were then washed in 96 vol% ethanol for 1 h and left to dry in the sterile atmosphere for 45 min followed by washing in medium (for spleen cells) or PBS (for L929 cell line or in vivo experiments) for 2 h at 4 °C.

## 2.3. Implant characterization

### 2.3.1. FTIR-ATR and SEM

FTIR-ATR analysis was conducted with Thermo Scientific Nicolet iS10 FTIR Spectrometer instrument equipped with Smart iTX ATR Diamond accessory. The spectra were recorded in

the range of 400-4000 cm$^{-1}$ with the resolution of 0.5 cm$^{-1}$ and then normalized to the highest peak intensity.

Microstructural properties of implant surfaces were examined with the field emission SEM (TESCAN MIRA 3 XMU). Before the recording, dry implant samples were cooled in liquid nitrogen, fractured and sputtered with carbon.

Dry implant samples were prepared for FTIR-ATR and SEM characterization using the solvent exchange drying protocol. Wet implant samples were dipped for 1 h in ethanol, then 1 h in heptane, and finally air-dried for at least 24 h at ambient temperature.

2.3.2. Mass swelling degree and water content

Before the experiment, the implant was equilibrated in PBS for 24 h. In the beginning, the mass of a wet implant specimen was measured. The specimen was subsequently dried in an oven at 100 °C for 2 h, and finally, the mass of the dry implant was determined. The experiment was performed in triplicate.

Mass swelling degree (MSD) was calculated based on the wet implant mass at time $t$, $m_t$, and the dry implant mass, $m_0$, measured at the end of the experiment, according to the following formula

$$MSD = 100 \cdot (m_t - m_0)/m_0 \ (\%) \tag{1}$$

Water content (WC) of the implant was calculated using the following equation

$$WC = 100 \cdot MSD/(100 + MSD) \ (\%) \tag{2}$$

2.3.3. Swelling kinetics

Swelling kinetics in PBS were monitored by measuring the MSD of the implant at predefined time intervals until the equilibrium MSD was achieved. Mass of the wet implant equilibrated in PBS was measured, and then the implant was air-dried at ambient temperature for 72 h. Dry mass of the implant was measured before the experiment. At the beginning of the experiment, the dry implant was immersed into the excess amount of PBS in a Petri dish.

After 2 min, the implant was taken out and carefully blotted using filter paper. Its wet mass was recorded, and the implant was immediately returned to the PBS solution. This procedure was repeated every 2 min until the equilibrium MSD was reached. Recording of the implant swelling kinetics was performed in triplicate.

2.3.4. Determination of carboxyl group concentration

Determination of carboxyl group concentration was carried out using the potentiometric acid-base titration method. One wet implant (about 40 mg of dry mass) was broken into pieces and immersed in 100 mL of 0.1 M HCl solution. The solution was stirred for 1 h to protonate all carboxyl groups in the sample and then the sample was thoroughly rinsed with distilled water. The protonated sample was subsequently submerged in 40 mL of 0.01 M NaOH solution, and the mixture was stirred again for 1 h in a capped beaker. The sample was then separated from the residual solution, rinsed with distilled water, dried for 2 h at 100 °C, and the dry mass of the sample was finally weighed. Two aliquots of 15 mL of residual solution were titrated with 0.01 M HCl, and the change in pH was monitored with a pH-meter (HI 3222, Hanna Instruments) to determine the equivalence point. As a blank probe, 15 mL of 0.01 M NaOH solution was titrated with 0.01 M HCl. The experiment was performed in duplicate.

The concentration of carboxyl groups (Ccg) was calculated according to the following expression

$$\mathrm{Ccg}(\mathrm{mmol\,g^{-1}}) = 0.4(1 - V_2/V_1)/W_{\mathrm{d}} \tag{3}$$

where $V_1$ is the volume of 0.01 M HCl solution consumed for the titration of the blank probe, $V_2$ is the volume of 0.01 M HCl solution consumed for the titration of the residual solution aliquot, and $W_{\mathrm{d}}$ is the mass of the dry sample.

2.3.5. Absorption of MB

A wet implant previously equilibrated in PBS was carefully blotted with tissue paper, and its wet mass was measured. The wet implant was then immersed in 25 mL of 1000 µg g$^{-1}$ MB

aqueous solution for 120 h. The molar amount of MB in the loading solution corresponded to the number of carboxyl groups measured for the implant ($n(MB^+)/n(-COOH) = 1$). MB absorption experiment was replicated three times.

## 2.3.6. The release of MB in vitro

Implant loaded with MB was rinsed with distilled water, and its surface was carefully blotted with a paper tissue. The prepared implant was subsequently immersed in 50 mL of PBS. The solution with the implant was kept at $37.0 \pm 0.1$ °C in the water bath during the MB release experiment. Aliquots of 3 mL were taken at predefined time intervals for 28 days to follow the release kinetics. Immediately after each sampling, the entire solution volume was replaced with the same volume of fresh PBS. Release kinetics were monitored with the UV-vis spectrophotometer (GBC Cintra 101) at the absorption wavelength of 664 nm. MB release experiments were performed in triplicate.

## 2.4. Biocompatibility tests

### 2.4.1. Cell culture

L929 mouse fibroblast cell line (the European Collection of Animal Cell Cultures) was grown in RPMI 1640 supplemented with 10% FCS and gentamycin at 37 °C in a humidified atmosphere with 5% $CO_2$. Following conventional trypsinization procedure, cells were seeded, with or without implants ($2 \times 10^4$ cells/well in a 24-well plate), and incubated during 1, 2, 4 and 24 h. At indicated times, cells were detached from plates/implants, and the cell suspension was kept the next 24 h in a 96-well plate (five replicates for each condition) and used for viability tests.

The spleen cells were isolated from male Dark Agouti rat (6 weeks old) as described previously.[19] Spleen tissue was mechanically disintegrated through a cell strainer (BD Falcon, BD Bioscience, Bedford, USA), and cells were resuspended in RPMI-1640 culture medium. Cell viability determined by Trypan blue dye (dye content ~40%) (Fluka, Sigma-

Aldrich, USA)  exclusion was larger than 90%. The isolated spleen cells ($0.5 \times 10^6$ cells mL$^{-1}$) were seeded in 24-well microtiter plates, with or without implants, and incubated for 24 and 48 h under standard conditions (5% $CO_2$, 37 °C).

### 2.4.2. Animal study

Male Dark Agouti rats (12-14 weeks old), conventionally housed at the Institute for Biological Research "Sinisa Stankovic" (IBISS), University of Belgrade, Serbia, were used in the pilot experiment. Experimental procedures were carried out in compliance with the Directive 2010/63/EU on the protection of animals used for experimental and other scientific purposes and were approved by the Ethical Committee of IBISS.

For implantation, animals were anesthetized by intraperitoneal administration of 40 mg kg$^{-1}$ of body weight of thiopental sodium (Rotexmedica, Tritau, Germany). The dorsum was clipped of hair, two incisions were made on either side of the dorsal midline, as described by Mirkov et al.[20], and one implant was aseptically implanted subcutaneously on each side of five rats. Control rats (n = 5) were sham-operated. Following the procedure, animals were housed individually for 1, 3 and 7 days post implantation (p.i.).

After 1, 3 and 7 days, rats were reanesthetized, and implants were quickly taken out through skin incisions. Overlying skin was taken for histological analysis and short-term culture of skin explants, as described by Popov Aleksandrov et al..[21] Blood was collected for complete blood tests analyses conducted using a Siemens ADVIA 120 flow cytometer (Terytown, N.Y., USA).

### 2.4.3. Cell activity tests

*MTT*: The metabolic activity of cells was assessed by MTT quantitative colorimetric assay.[22] After cultivation in the absence or presence of implants, 0.5 mg mL$^{-1}$ MTT was added to L929 and spleen cells and incubated for 2 h at 37 °C. Formazan was dissolved by overnight incubation in 10% sodium dodecyl sulfate (Merck-Schuchardt, Germany) (SDS)-0.01 N HCl. Absorbance was measured spectrophotometrically at 540/650 nm, by an Enzyme-linked

immunosorbent assay (ELISA) 96-well plate reader (GDV EC, Roma, Italy). Skin cell viability was also determined by MTT reduction assays, as described by Popov Aleksandrov et al..[21] The skin was cut into small pieces and placed in wells of 96-well plates. MTT was added (0.5 mg mL$^{-1}$), and the skin was incubated for 3 h. Produced formazan was dissolved by overnight incubation of skin explants in 2-methoxyethanol (Fluka AG, Buchs SG, Switzerland) and evaluated spectrophotometrically.

*Crystal violet*: Cell adhesion was evaluated with a Crystal violet assay. L929 cells were washed in PBS and fixed with glutaraldehyde (Sigma) (2.5 vol%) at 4 °C for 20 min, then stained with crystal violet (1%) for 30 min. After washing with tap water, crystal violet was solubilized with 0.5% SDS, and the absorbance was measured spectrophotometrically at 540/650 nm, by an ELISA 96-well plate reader.

*NO*: For NO production, cells isolated from spleen ($1 \times 10^6$/well) were grown in complete RPMI-1640 medium with or without ConA (1 µg mL$^{-1}$) in 96-well plates for 48 h, and NO level was measured using Griess reaction, as described elsewhere.[23] NO levels were also measured in conditioned media of skin explants.

*ELISA*: Levels of tumor necrosis factor-α (TNF-α) and interleukin-6 (IL-6) in serum or media conditioned by skin explants for 48 h were determined with ELISAs for rat TNF-α (eBioscience Inc., San Diego, CA) and rat IL-6 (R&D systems, Minneapolis, MN) according to manufacturer's instructions.

## 2.4. Statistical analysis

All quantitative data were reported as a mean ± standard deviation (SD) of the sample from the number of experiments indicated individually for each of the used methods. Results of in vitro experiments with cells (all samples were set in five replicates) and in vivo experiments (with four animals assigned to each experimental group) were expressed as mean ± SD and statistical analysis was performed using STATISTICA 7.0 (StatSoft Inc., Tulsa, OK).

Statistical significance was defined by a Mann-Whitney U test and *P*-values less than 0.05 were considered as significant.

## 3. Results and Discussion

### 3.1. FTIR-ATR characterization

**Figure 1**a shows the spectra of the pure polymer base and implant dried by solvent exchange. Several absorption bands are prominent in the DL-PLCL spectrum: symmetrical valence vibrations of C-O-C in the aliphatic chain at 1093 cm$^{-1}$, symmetric C-O-C stretching at 1161 cm$^{-1}$, asymmetric C-H bending in CH$_3$ at 1453 cm$^{-1}$, C=O stretching at 1732 cm$^{-1}$, and the CH$_2$ stretching bands at 2867 cm$^{-1}$ and 2940 cm$^{-1}$. Absorption bands indicating the presence of PAA in dry implant are the C-O stretching bands at 1404 cm$^{-1}$ and 1560 cm$^{-1}$, and the O-H stretching band at 3384 cm$^{-1}$. The absorption bands corresponding to the pure DL-PLCL or PAA components are not shifted indicating a physical blending of separated phases without the formation of new chemical bonds. Figure 1b depicts spectra of dry and wet implants. The new absorption band at 1637 cm$^{-1}$ in wet implant spectrum corresponds to the hydrogen bonding of carboxyl groups. The dominant absorption band with the highest intensity in this spectrum is the O-H stretching band at 3384 cm$^{-1}$. Both these bands are common indicators of PAA hydrogel formation.

**(Figure 1)**

### 3.2. SEM characterization

SEM images of the surface and cross section of the implant are shown in **Figure 2**. The heterogeneous microstructure of the implant comprises a continuous DL-PLCL polymer matrix filled with PAA hydrogel inclusions. The marked difference in hydrogel distribution can be observed between the surface and cross section. Sparsely dispersed isolated aggregates of irregular PAA particles with the average cluster size of about 1.1 μm can be observed at the

surface. Throughout the cross section, spheroidal PAA particles with a mean diameter of around 280 nm are uniformly and densely packed within the DL-PLCL matrix. Hydrogel particles appear to be attached to the polymeric support in both regions.

**(Figure 2)**

The microstructure of the composite implant results from the complex interplay of phenomena occurring during the fabrication process. Photoirradiation by UV light triggers polymerization and cross-linking of AA initiating the phase separation, as confirmed by solution hazy appearance. After the immersion and solidification in the PBS bath, discs turned white and formed hydrogel-filled composite implants. Aqueous environment imposes unstable thermodynamic conditions leading to the completion of phase separation between the hydrophilic cross-linked PAA hydrogel-rich phase and the hydrophobic DL-PLCL polymer-rich phase. Hydrogel-rich phase is dispersed throughout the implant volume in the form of submicron size particles and their aggregates close to the surface, while the DL-PLCL-rich phase acts as the surrounding matrix. Polymer gels commonly exhibit locally nonuniform spatial distributions of polymer network concentration and cross-linking density.[24] Formation of small hydrogel particles or their isolated aggregates can be explained by the higher rate of polymerization achieved with the trifunctional cross-linker TMPTA in comparison with the monofunctional AA monomer. Hence, microgels are formed after the cross-linker depletion in the system.  The surface of the composite implant has a lower hydrogel content compared to the bulk. The mechanism by which this surface layer is created is similar to the mechanism of skin formation in membrane fabrication by immersion precipitation.[25] Immediately after the immersion into the PBS bath, NMP is quickly depleted from the irradiated disc while the PBS solution slowly penetrates towards the interior. Such a phenomenon leads to the formation of a skin layer enriched in DL-PLCL with embedded sparsely dispersed aggregates of PAA-rich phase.

### 3.3. Basic properties (MSD, WC, and Ccg) and swelling kinetics

Implant formulation comprised 16 wt% of DL-PLCL and 20 wt% of AA and cross-linker. The concentration of TMPTA was 10 mol%. The basic properties of the obtained implants are listed in **Table 1**.

**(Table 1)**

Implants exhibit a moderate swelling degree and good ion-exchange capacity. Measurements of the basic parameters have very low SDs indicating a robust method of implant preparation that yields high reproducibility. MSD of the composite implant is significantly lower compared to the values for pure PAA hydrogel in PBS solution.[11] Such a result is expected because the DL-PLCL polymeric base limits PAA hydrogel swelling and improves the mechanical stability of the implants. High WC of the implant equilibrated in PBS reveals the predominant hydrophilic nature of the implant that commonly indicates better biocompatibility and reduced inflammatory response.[26] Value of Ccg is comparable to a typical ion-exchange resin.

**Figure 3** shows that the implant retains disc geometry during the drying and swelling and that MSD reaches its equilibrium value after about 6 min.

**(Figure 3)**

Swelling within few minutes was previously reported only for superporous hydrogels (SPHs).[27] SPHs are hydrophilic polymer networks able to quickly imbibe vast amounts of water because of a structure containing interconnected microscopic pores that allow capillary action.[28] Our composite implant is not a porous structure, but rather contains closely packed microgel particles within the hydrophobic polymer matrix.

Swelling kinetics of the implant seems to be well described by the Boltzmann (sigmoidal) function. Initial lag in swelling shown in Figure 3b can be explained by the skin layer with lower hydrogel content, which acts as a barrier to the penetration of PBS. PAA-rich microgel

particles in the interior swell rapidly as a result of their small size and strongly hydrophilic surface. After the swelling of surface hydrogel aggregates, implant surface becomes negatively charged and electrostatically attracts buffer cations. The high density of negative charges in the swollen state and dense packing of interior microgel particles further increase the rate of cation penetration and hydrogel formation.

Equilibrium MSD established in PBS after one cycle of air drying at ambient temperature is nearly the same as the initial MSD, which indicates implant capability of reversible swelling. Reversible swelling and fast swelling kinetics of the composite implant can facilitate the use and storage of the implant in the clinical setting. Implants can be stored and transported in the dry state after the drug is loaded. Before the application, the composite implant can be quickly rehydrated and used at the point of care.

### 3.4. Studies of MB absorption and release in vitro

The composite implant exhibited excellent loading efficiency of $95.8 \pm 0.4\%$ after MB absorption implying that excessive amount of MB in the absorption solution was not required. A total of $85.1 \pm 1.8\%$ of the loaded MB amount was released in the PBS solution at the end of the in vitro release experiments at 37 °C, while the residual amount of about 15% remained bound to the implant. The ratio of the released and bound fractions of MB gives the approximate ratio of MB amounts bound by electrostatic and hydrophobic forces, respectively. Relative cumulative amount of released MB $Q_t/Q_e$ is presented as a function of $t^{0.5}$ in **Figure 4**.

**(Figure 4)**

Concentrations of released MB at time $t$, $Q_t$, were normalized to the equilibrium concentration of released MB, $Q_e$, reached at the end of the experiment. The release kinetics of MB exhibits Fickian behavior which extends even to longer times. The released amount is diffusion-controlled and easy to predict in the initial period of around 14 days. The calculated apparent diffusion coefficient was $D_a = 3.54 \times 10^{-13}$ m$^2$ s$^{-1}$ (**Appendix 1** and **Appendix 2**).

MB release kinetics from the composite implant can be well described as a diffusion-controlled process. Such description is suitable for the given experimental conditions because the diffusive transport of MB through the hydrogel-rich phase of the implant proceeds significantly slower compared to the rate of electrostatic interactions involved in MB release. Because of the monolithic structure of the reservoir, constant $D_a$ is an adequate parameter for the characterization and prediction of the release kinetics.

Value of $D_a$ for the composite reservoir calculated from experimental data is about two orders of magnitude lower than the diffusion coefficient reported for MB in free poly(ethylene glycol) diacrylate hydrogels.[29] The following arguments could address this discrepancy. Thin surface layer with reduced hydrogel content could act as an effective rate-limiting barrier for MB diffusion. Additionally, the effective pore size between the hydrogel chains for cross-linked PAA hydrogel is probably much smaller than that of the referenced poly(ethylene glycol) diacrylate hydrogels having a high concentration of cross-links that impose steric restrictions. We estimated the average pore diameter of cross-linked PAA hydrogel to be 2.62 nm (**Appendix 3**) which is quite close to MB molecular size reported as 0.591 nm × 1.382 nm.[30] Both the structure of the surface layer and effective pore size, which control the release kinetics, could be modified by changing the compositions of the starting solution and nonsolvent bath used for implant preparation.

### 3.5. Implant biocompatibility in vitro

Mouse fibroblast cell line L929 was used for cytotoxicity evaluation of the implants, as is routinely carried out in biomaterials research.[31,32] **Figure 5**a shows that the metabolic activity of L929 cells assessed by MTT reduction assay decreased in samples incubated with implants after 1 h of cultivation, compared to the control samples without implants. Additionally, Crystal violet test indicated lower adhesion potential of cells cultivated with implants at all times, as seen in Figure 5b.

**(Figure 5)**

L929 cell line is a continuous adherent cell line, and its ability to adhere influences cell morphology and capacity to proliferate and differentiate.[32] Therefore, the observed lack of adhesion could be responsible for decreased MTT reduction capability of the cells with implants 2 h following incubation, compared to the control. Khorasani et al.[33] showed that hydrophobic and a more negative surface charge of biomaterials impaired the L929 cell membrane adhesion capacity, which could affect cell membrane function, and lead to decreased metabolic activity. These observations are in line with our results as the implants were negatively charged (carboxyl groups). A study of endothelial cell incubation on different functionalized surfaces also confirmed that surface carboxyl groups led to the decrease in cell attachment and growth.[34]

Primary cells were isolated from the spleen of the rat and cultured in the presence of implants for 24 and 48 h to investigate further the cytotoxic effects of implants. As shown by Trypan blue assay results in **Figure 6**a, the implants did not affect cell viability. However, Figure 6b shows that the MTT test results indicated a significantly higher metabolic activity in samples with implants following 48 h of incubation. MTT reduction following 48 h after incubation is in line with other studies showing the stimulatory potential of biomaterials on cell metabolic/mitochondrial functions.[32,35] The apparent discrepancy in MTT reduction potential between L929 cell line and splenocytes could be explained by the difference in the functional aspects of these two cell types and their distinct origin and requirements. Apart from the fact that adhesion is a limiting step in L929 cells activity, these cells could be more sensitive to biomaterials compared to primary cells.[31]

**(Figure 6)**

Along with cytotoxicity, the potential of biomaterial to elicit an inflammatory reaction is also an important aspect in biocompatibility assessments. We observed lower levels of NO in supernatants of cells incubated with implants compared to the control, thus demonstrating no proinflammatory effect of the biomaterial on spleen cells. Moreover, as depicted in Figure 6c,

a diminished response to ConA stimulation implies the immunosuppressive potential of implants. NO is a well-known inflammatory mediator[36] and its reduction by splenocytes cultivated with implants indicates the lack of direct proinflammatory potential of implants compared to the control. Additionally, splenocytes cultured with implants failed to respond to stimulation with common lymphocyte mitogen ConA, which highlights the suppressive effect of implants on basic proinflammatory pathways in vitro.

### 3.6. Implant biocompatibility in vivo

A rat model of subcutaneous implant installation was used to obtain initial information concerning the biocompatibility of these new materials through the pilot in vivo study. Regarding systemic effects, peripheral blood parameters – differential leukocyte counts and biochemical parameters (**Table S1**, Supporting Information), we observed a drop in total leukocyte numbers and percentage of neutrophils on days 1 and 3 p.i., a statistically significant increase in percentages of mononuclear cells, eosinophils, and basophils on day 1, and a decrease in platelet count, between sham-operated and implanted rats. On day 7 p.i., a statistically significant drop in the percentage of monocytes, as well as an increase in eosinophils were noted in implanted rats. Slight differences in the drop of leukocyte numbers on account of neutrophils on days 1 and 3 p.i. imply the recruitment of these early immune responders into the skin area around the implant. Increased percentage of monocytes, eosinophils, and basophils could represent a transient inflammatory response to the implant. Although elevated numbers of eosinophils could reflect an allergic property of implants, their presence, however, might be perceived as homeostatic/immunoregulatory.[37]

Levels of proinflammatory cytokines TNF-α and IL-6 in the serum of all rats were below the level of method detection. Judged by the undetectable levels of these innate immune proinflammatory cytokines in the serum of implanted rats, the implanted material caused no systemic proinflammatory reaction.

Histological examination of skin overlying the implants and skin from sham-operated rats showed edematous, loose connective tissue in both animal groups on day 1 but with more compact clusters of cell debris and young connective tissue (pseudocapsule in formation) in the group of animals with implants as illustrated in **Figure 7**a,b. Time-dependent connective tissue formation/organization characteristic for pseudocapsule formation was seen in this group of animals, with more edematous connective tissue in the group with implants at day 7 as compared to more compact cellular connective tissue (early phase of scar formation) in the skin of sham-implanted rats as shown in Figure 7c,d. No cell infiltration into implants was observed (**Figure S2**, Supporting Information).

**(Figure 7)**

Formation of fibrous capsule represents a normal host response to a foreign body, but the slower formation of scar tissue in the skin of implanted individuals is an indication of slower wound healing that might be ascribed to properties of the implant surface. Wet implant surface exhibits a high concentration of hydrophilic and negatively charged carboxyl groups that may reduce protein adsorption and partially inhibit cell growth, as reviewed in Tang et al..[38]

Regarding local skin activity response to the foreign material, metabolic activity increased in skin explants from implanted animals at all times (except 0 h first day and 24 h seventh day p.i.), as illustrated in **Figure 8**a. The increase of MTT reduction by skin explants, in compliance with our in vitro studies on splenocytes, could reflect the increased proliferative activity of epithelial cells attempting to protect the vulnerable skin area.

**(Figure 8)**

As Figure 8b shows, NO production by skin explants from implanted rats increased on day 1 p.i. and then returned to the basal level. This increased production of NO by skin explants could be responsible for impaired wound healing as NO is, apart from being an early

inflammatory marker, also known as a signaling molecule that prevents thrombosis by inhibiting platelets activation.[39] Alternatively, it might be viewed as the host attempt to stimulate wound healing, given the important role of this mediator in the healing process.[40] As Figure 8c shows, there was no difference in TNF-α and IL-6 production by skin explants between control and implanted rats. Similar production of these cytokines by skin explants in implanted and sham-operated rats further suggests the absence of proinflammatory effect. General lack of the effect of implants on inflammatory cytokine production illustrates their low toxicity to the covering skin.

## 4. Conclusions

We presented a simple and robust synthesis method for the fabrication of implantable DL-PLCL/PAA composite reservoirs for cationic drugs. The implants exhibited good ion-exchange capacity, moderate swelling degree and the capability for fast reversible swelling within a few minutes while retaining the original geometry. In vitro drug loading and release experiments using MB as the model drug showed excellent loading efficiency and diffusion-controlled release kinetics during two weeks.

Biocompatibility of the unloaded reservoirs was examined through a series of in vitro tests and a pilot experiment in vivo. Implants exhibited low toxicity in vitro and in vivo, while the in vivo acute response analysis showed a normal foreign body reaction and early stages of slow fibrous capsule formation, which is beneficial for controlled drug delivery over longer periods. Interaction of the unloaded reservoir with the biological environment is mainly determined by the presence of free carboxyl groups on the surface that makes the surface highly hydrophilic and negatively charged. However, implantable reservoirs loaded with cationic drugs are expected to have different time-dependent surface properties, and their biocompatibility is one of the crucial topics for our future research.

Obtained implantable composite drug reservoirs could serve as a versatile tool for controlled delivery of cationic drugs. Key implant properties relevant for drug delivery can be tuned

already in the synthesis stage through the modifications of the precursor solution composition and mold geometry. Some additional modifications of implant properties will be investigated in the future to suppress fibrous capsule formation and improve their performance over longer time periods.

## Supporting Information

Supporting Information is available from the Wiley Online Library or from the author.

## Appendix 1. Model of drug diffusion from monolithic cylindrical reservoirs

When the drug is dissolved within the monolithic carrier matrix, it exists in the form of a solution where drug molecules are nearly uniformly distributed in the reservoir material. The rate of drug release by diffusion from monolithic reservoirs is influenced by reservoir geometry.[41] Release kinetics controlled by diffusion through the reservoir of cylindrical geometry can be described by[42]

$$\frac{M_t}{M_\infty} = 1 - \frac{32}{\pi^2}\sum_{n=1}^{\infty}\frac{1}{q_n^2}\exp\left(-\frac{q_n^2}{R^2}D_a t\right) \times \sum_{p=0}^{\infty}\frac{1}{(2p+1)^2}\exp\left(-\frac{(2p+1)^2\pi^2}{H^2}D_a t\right) \qquad (A1)$$

where $M_t$ and $M_\infty$ are the cumulative amounts of released drug at time $t$ and infinity (or equilibrium), respectively; $n$ and $p$ are the dummy summation variables; $q_n$ are the roots of the Bessel function of the first kind and zero order ($J_0(q_n) = 0$), $R$ is the cylinder radius, $H$ is the cylinder height, and $D_a$ is the apparent diffusion coefficient. The analytical expression in Equation (A1) converges quite slowly for small times and requires a large number of series terms to be numerically evaluated with acceptable accuracy. Very good approximation of the analytical expression for small times adequate for numerical evaluation is given by the expansion[43]

$$\frac{M_t}{M_\infty} =$$

$$\left(\frac{D_a t}{L^2}\right)^{0.5}\left[\frac{2}{\pi^{0.5}}+\frac{4}{\pi^{0.5}}\left(\frac{L}{R}\right)\right]-\frac{D_a t}{L^2}\left[\frac{8}{\pi}\left(\frac{L}{R}\right)+\left(\frac{L}{R}\right)^2\right]+$$

$$\left(\frac{D_a t}{L^2}\right)^{1.5}\left[\frac{2}{\pi^{0.5}}\left(\frac{L}{R}\right)^2-\frac{1}{6\pi^{0.5}}\left(\frac{L}{R}\right)^3\right]+\left(\frac{D_a t}{L^2}\right)^2\left[\frac{1}{3\pi}\left(\frac{L}{R}\right)^3-\frac{1}{8}\left(\frac{L}{R}\right)^4\right]+\cdots$$

$$(A2)$$

where *L* is half of the cylinder height *H*. For small values of *L/R*, the first four terms of the expansion already provide sufficient accuracy in most cases. If we assume that *L/R* = 0, the expression is reduced to the small time approximation for the plane sheet which can also be used as an approximation for very thin disks.

$D_a$ can be evaluated from experimental data via nonlinear regression by applying the gradient descent optimization algorithm. Approximation for small times expressed as appropriately truncated expansion may be used as a regression model with good accuracy.


## Appendix 2. Calculation of $D_a$ of the composite reservoir

$D_a$ was determined from nonlinear regression by applying the gradient descent optimization algorithm with two variable parameters: $D_a$ as the presumably constant apparent diffusion coefficient and *b* as the ordinate intercept. Through independent iterative variations of $D_a$ and *b* with fixed steps, the sum of squared errors was minimized. As the regression model, we used the expression

$$\frac{M_t}{M_\infty} =$$

$$\left(\frac{D_a t}{L^2}\right)^{0.5}\left[\frac{2}{\pi^{0.5}}+\frac{4}{\pi^{0.5}}\left(\frac{L}{R}\right)\right]-\frac{D_a t}{L^2}\left[\frac{8}{\pi}\left(\frac{L}{R}\right)+\left(\frac{L}{R}\right)^2\right]+$$

$$\left(\frac{D_a t}{L^2}\right)^{1.5}\left[\frac{2}{\pi^{0.5}}\left(\frac{L}{R}\right)^2-\frac{1}{6\pi^{0.5}}\left(\frac{L}{R}\right)^3\right]+\left(\frac{D_a t}{L^2}\right)^2\left[\frac{1}{3\pi}\left(\frac{L}{R}\right)^3-\frac{1}{8}\left(\frac{L}{R}\right)^4\right]+b$$

$$(A3)$$

which was applied to the region of six initial experimental time points. The values of $L = 0.629$ mm and $R = 6.5$ mm were determined from initial weights of the wet implants loaded with MB and measurements with a liner. The initial value of $D_a = 2.815 \times 10^{-13}$ m$^2$ s$^{-1}$ was determined from the slope of linear fit shown in Figure 4 assuming thin disk approximation for the implant geometry. The initial value of $b = 0$ was chosen assuming no additional barriers to diffusion. Calculated values obtained by this algorithm were $D_a = 3.54 \times 10^{-13}$ m$^2$ s$^{-1}$ and $b = -0.259$ with the adjusted coefficient of determination $R^2 = 0.9971$. Comparison of the experimental data and the fitted curve is illustrated in **Figure A1**. Code of the algorithm (**MATLAB script: calculation of $D_a$ for cylindric composite reservoir geometry**, Supporting Information) was written in the MATLAB programming package (MATLAB R2016b, The MathWorks, Inc., Natick, Massachusetts, United States). The implemented algorithm converged successfully (**Figure S1**, Supporting Information).

**(Figure A1)**

## Appendix 3. Pore size estimation of the composite reservoir

An estimate of the pore size of the composite reservoir was made via the gel correlation length model. Estimation of the correlation length was performed according to the PAA gel correlation length model explained in detail by Hu and Dickson (see[44] and references therein). Mean mesh size between the interchain crossings $\xi$ is designated as the correlation length with the assumption that $\xi$ equals the effective reservoir pore diameter. $\xi$ can be evaluated using the following expressions

$$\xi \cong \left( L_B + \frac{1}{16\pi l_B A_C c} \right)^{-\frac{1}{4}} (4\pi A_C c)^{\frac{1}{8}} (A_C c)^{-\frac{3}{4}} \qquad (A4)$$
$$c = \frac{A_V \phi}{v M_W} \qquad (A5)$$

where $L_B$ is the bare persistence length, $l_B$ is the Bjerrum length, $A_C$ is the contour distance of two adjacent charge groups along the polymer chain, $c$ is the concentration of the charged

segments, $A_V$ is the Avogadro constant, $\phi$ is the PAA gel volume fraction, $v$ is the partial specific volume of the PAA gel in the reservoir, and $M_W$ the molecular weight of the monomer.

PAA gel volume fraction $\phi$ was calculated via the expression from the studies of Zhou and coworkers (see[45] and references therein)

$$\phi = \frac{(m_d - m_0)v}{V - m_0/\rho_{DL-PLCL}} \tag{A6}$$

where $m_d$ is the dry mass of the reservoir sample, $m_0$ mass of the nascent DL-PLCL substrate, $V$ the reservoir sample volume, and $\rho_{DL\text{-}PLCL}$ the mass density of DL-PLCL.

Pore diameter values were extrapolated from the graph in **Figure 4** of the reference[44] using linearization and extension of the log-log plot. For the unloaded reservoirs in the swollen state (equilibrated in PBS at pH $= 7.4$ and $I = 0.154$ M), the obtained effective mean pore diameter is 2.62 nm. The estimated mean pore diameter is reduced to 2.22 nm for the reservoirs loaded with MB.

[1]     A. Kumar, J. Pillai, In *Nanostructures for the Engineering of Cells, Tissues and Organs: From Design to Applications*, (Ed.: A. M. Grumezescu), Elsevier Science, **2018**, Ch. 13.

[2]     L. Claes, A. Ignatius, *Chirurg* **2002**, *73*, 990.

[3]     H. Tian, Z. Tang, X. Zhuang, X. Chen, X. Jing, *Prog. Polym. Sci.* **2012**, *37*, 237.

[4]     J. Li, D. J. Mooney, *Nat. Rev. Mater.* **2016**, *1*, 1.

[5]     N. J. Shah, M. N. Hyder, M. A. Quadir, N.-M. Dorval Courchesne, H. J. Seeherman, M. Nevins, M. Spector, P. T. Hammond, *Proc. Natl. Acad. Sci. U. S. A.* **2014**, *111*, 12847.

[6]     M. L. Macdonald, R. E. Samuel, N. J. Shah, R. F. Padera, Y. M. Beben, P. T. Hammond, *Biomaterials* **2011**, *32*, 1446.

[7]     S. Gupta, P. Benien, P. K. Sahoo, *Curr. Drug Deliv.* **2010**, *7*, 252.

[8]     D. P. Elder, *J. Chem. Educ.* **2005**, *82*, 575.

[9]     M. Vuorio, J. A. Manzanares, L. Murtomäki, J. Hirvonen, T. Kankkunen, K. Kontturi, *J. Control. Release* **2003**, *91*, 439.

[10]    S. Kamath, D. Bhattacharyya, C. Padukudru, R. B. Timmons, L. Tang, *J. Biomed. Mater. Res. Part A* **2008**, *86A*, 617.

[11]    E. Jabbari, J. Tavakoli, A. S. Sarvestani, *Smart Mater. Struct.* **2007**, *16*, 1614.

[12]    O. Okay, In *Hydrogel Sensors and Actuators. Springer Series on Chemical Sensors and Biosensors (Methods and Applications),* Vol. 6 (Eds: G. Gerlach, K.-F., Arndt) Springer, Berlin, Heidelberg, Germany **2009**, Ch. 1.

[13] L. Guo, G. Liu, R. Y. Hong, H. Z. Li, *Mar. Drugs* **2010**, *8*, 2212.

[14] Abdel-Mohdy, A. Abou-Okeil, S. El-Sabagh, S. M. El-Sawy, *Int. J. Chem. Mol. Eng.* **2015**, *9*, 1149.

[15] K. S. Stankevich, N. V. Danilenko, R. M. Gadirov, S. I. Goreninskii, S. I. Tverdokhlebov, V. D. Filimonov, *Mater. Sci. Eng. C* **2017**, *71*, 862.

[16] Ž. Janićijević, F. Radovanović, *Polymer (Guildf).* **2018**, *147*, 56.

[17] Y. Fumimoto, A. Matsuyama, H. Komoda, H. Okura, C. M. Lee, A. Nagao, T. Nishida, T. Ito, Y. Sawa, *Tissue Eng. Part C Methods* **2009**, *15*, 437.

[18] M. Mulder, *Basic Principles of Membrane Technology*, 2nd ed., Kluwer Academic Publishers, Dordrecht **1996**, pp. 77–81.

[19] M. Ninkov, A. Popov Aleksandrov, I. Mirkov, J. Demenesku, D. Mileusnic, S. Jovanovic Stojanov, N. Golic, M. Tolinacki, L. Zolotarevski, D. Kataranovski, I. Brceski, M. Kataranovski, *Food Chem. Toxicol.* **2016**, *96*, 11.

[20] I. Mirkov, A. Popov Aleksandrov, J. Demenesku, M. Ninkov, D. Mileusnic, D. Kataranovski, M. Kataranovski, *Cutan. Ocul. Toxicol.* **2017**, *36*, 283.

[21] A. Popov Aleksandrov, M. Tusup, I. Mirkov, J. Djokic, M. Ninkov, L. Zolotarevski, D. Kataranovski, M. Kataranovski, *Cutan. Ocul. Toxicol.* **2015**, *34*, 149.

[22] F. Denizot, R. Lang, *J. Immunol. Methods* **1986**, *89*, 271.

[23] J. B. Hibbs, R. R. Taintor, Z. Vavrin, E. M. Rachlin, *Biochem. Biophys. Res. Commun.* **1988**, *157*, 87.

[24] E. S. Matsuo, M. Orkisz, S. T. Sun, Y. Li, T. Tanaka, *Macromolecules* **1994**, *27*, 6791.

[25] J. G. Wijmans, J. P. B. Baaij, C. A. Smolders, *J. Memb. Sci.* **1983**, *14*, 263.

[26] A. Hezi-Yamit, C. Sullivan, J. Wong, L. David, M. Chen, P. Cheng, D. Shumaker, J. N. Wilcox, K. Udipi, *J. Biomed. Mater. Res. Part A* **2009**, *90A*, 133.

[27] R. A. Gemeinhart, C. Guo, In *Reflexive polymers and hydrogels: understanding and designing fast responsive polymeric systems*, (Eds: N. Yui, R. J. Mrsny, K. Park), CRC

Press, Boca Raton, FL, USA **2004**, Ch. 13.

[28]   N. Vishal Gupta, H. G. Shivakumar, *DARU, J. Pharm. Sci.* **2010**, *18*, 200.

[29]   S. M. Evans, A. L. Litzenberger, A. E. Ellenberger, J. E. Maneval, E. L. Jablonski, B. M. Vogel, *Mater. Sci. Eng. C* **2014**, *35*, 322.

[30]   J. de S. Macedo, N. B. da Costa Júnior, L. E. Almeida, E. F. da S. Vieira, A. R. Cestari, I. de F. Gimenez, N. L. Villarreal Carreño, L. S. Barreto, *J. Colloid Interface Sci.* **2006**, *298*, 515.

[31]   B. Thonemann, G. Schmalz, K.-A. Hiller, H. Schweikl, *Dent. Mater.* **2002**, *18*, 318.

[32]   M. C. Serrano, R. Pagani, M. Vallet-Regí, J. Peña, A. Rámila, I. Izquierdo, M. T. Portolés, *Biomaterials* **2004**, *25*, 5603.

[33]   M. T. Khorasani, S. MoemenBellah, H. Mirzadeh, B. Sadatnia, *Colloids Surfaces B Biointerfaces* **2006**, *51*, 112.

[34]   H.-B. Lin, W. Sun, D. F. Mosher, C. García-Echeverría, K. Schaufelberger, P. I. Lelkes, S. L. Cooper, *J. Biomed. Mater. Res.* **1994**, *28*, 329.

[35]   A. G. Karakecili, T. T. Demirtas, C. Satriano, M. Gümüsderelioglu, G. Marletta, *J. Biosci. Bioeng.* **2007**, *104*, 69.

[36]   G. Cirino, E. Distrutti, J. Wallace, *Inflamm. Allergy-Drug Targets* **2006**, *5*, 115.

[37]   H. Kita, *Immunol. Rev.* **2011**, *242*, 161.

[38]   L. Tang, P. Thevenot, W. Hu, *Curr. Top. Med. Chem.* **2008**, *8*, 270.

[39]   J. W. Yau, H. Teoh, S. Verma, *BMC Cardiovasc. Disord.* **2015**, *15*, 130.

[40]   J. Luo, A. F. Chen, *Acta Pharmacol. Sin.* **2005**, *26*, 259.

[41]   J. Siepmann, F. Siepmann, *Int. J. Pharm.* **2008**, *364*, 328.

[42]   J. M. Vergnaud, *Controlled Drug Release of Oral Dosage Forms*, 1st ed., Ellis Horwood Limited, Chichester **1993**, pp. 75–104.

[43]   C. W. J. Nestor, *Diffusion from solid cylinders*, ORNL/CSD/TM-84, Oak Ridge National Laboratory, Oak Ridge, TN, USA, **1980**.

[44]  K. Hu, J. M. Dickson, *J. Memb. Sci.* **2008**, *321*, 162.

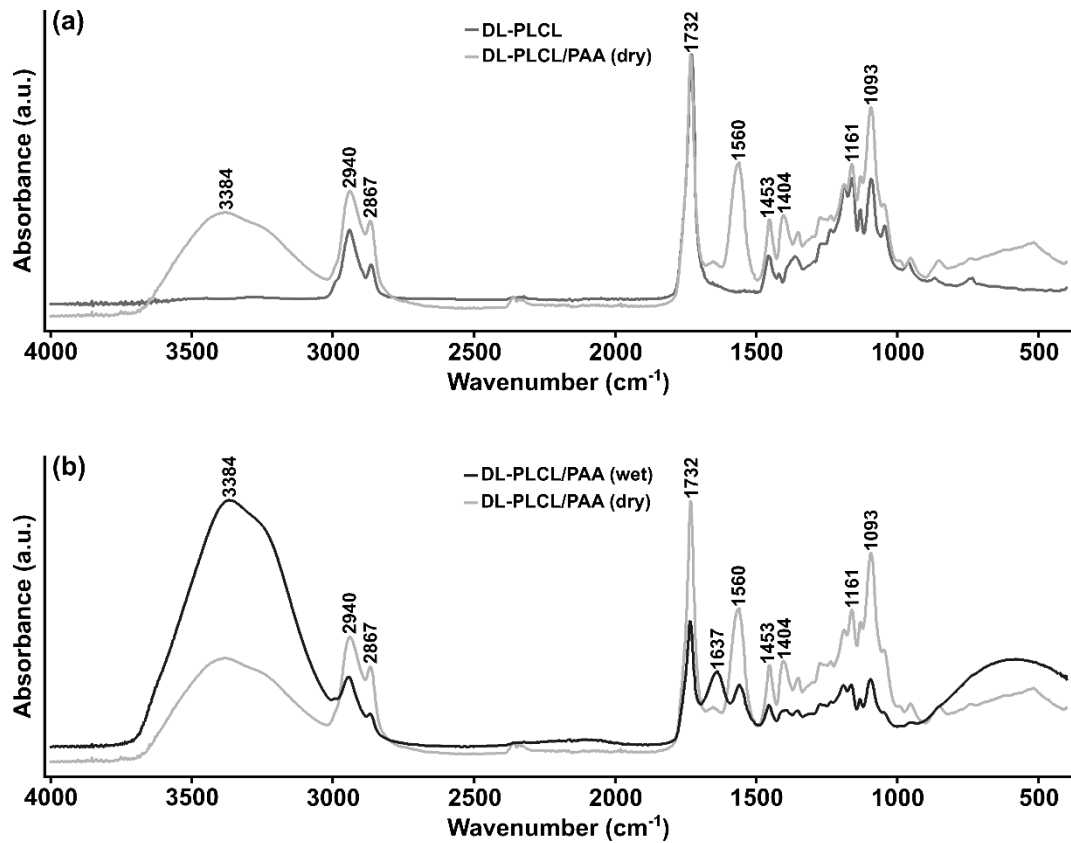[45]  J. Zhou, R. F. Childs, A. M. Mika, *J. Memb. Sci.* **2005**, *260*, 164.

*Figure 1.* FTIR-ATR spectra of (a) the pure polymer base (DL-PLCL) and dry implant (DL-PLCL/PAA (dry)) and (b) dry (DL-PLCL/PAA (dry)) and wet (DL-PLCL/PAA (wet)) implant.
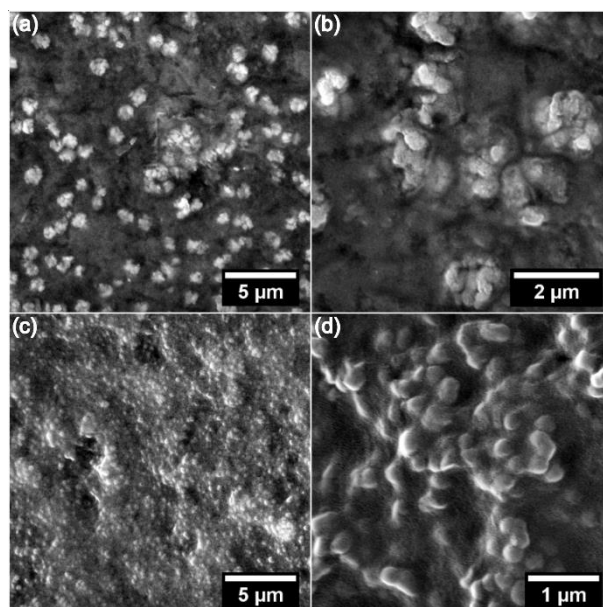
*Figure 2.* SEM images of the implant prepared from the casting solution composition with 16 wt% DL-PLCL, 3.41 mmol g$^{-1}$ AA, and 10 mol% TMPTA: implant surface ((a) and (b)) and implant cross section ((c) and (d)).
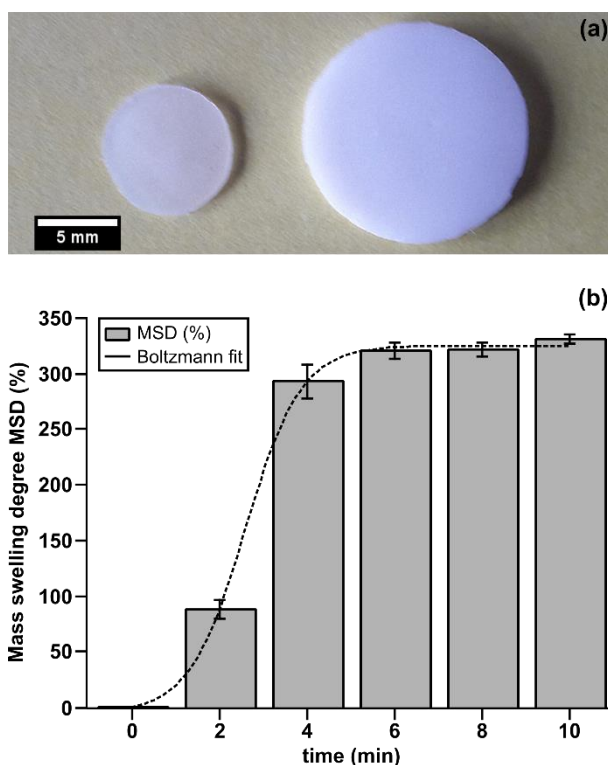


*Figure 3.* Swelling of the composite implant: (a) shape of the dry implant (left) and wet implant equilibrated in PBS (right); (b) swelling kinetics and the fitted sigmoidal dependence using the Boltzmann function. Error bars correspond to the ± SD.
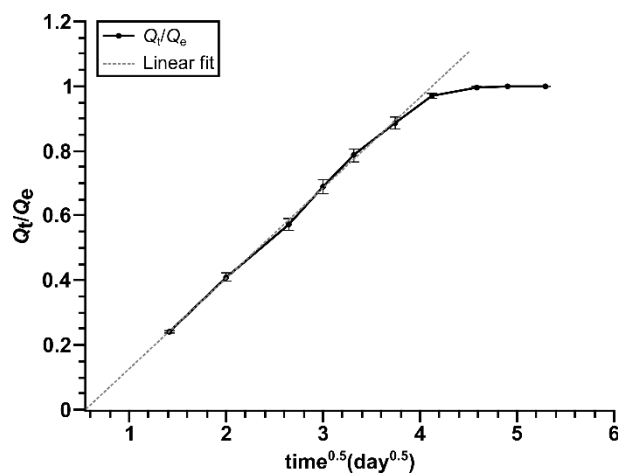


*Figure 4.* The release of MB in PBS buffer at 37 °C presented as a relative cumulative amount of released MB ($Q_t/Q_e$) versus square root of time ($t^{0.5}$) to illustrate the diffusion-controlled kinetics.
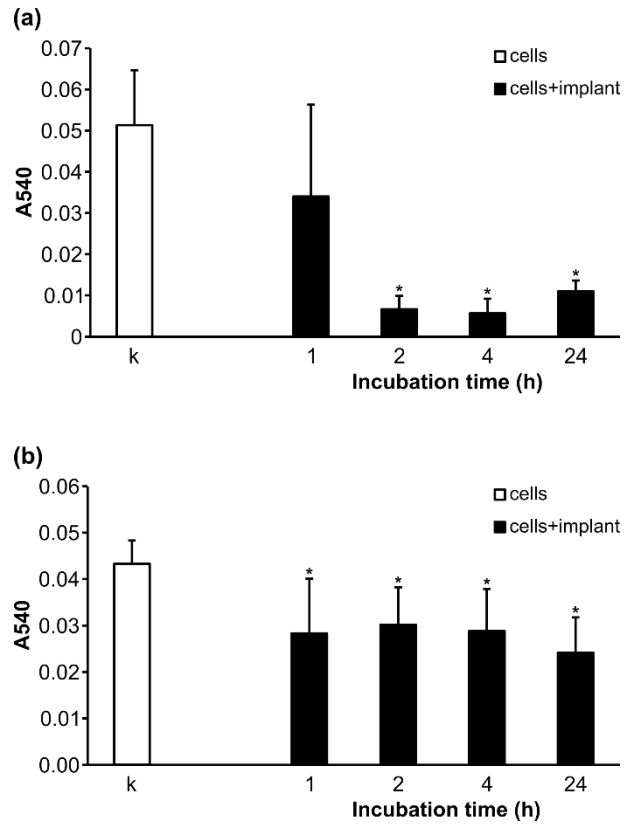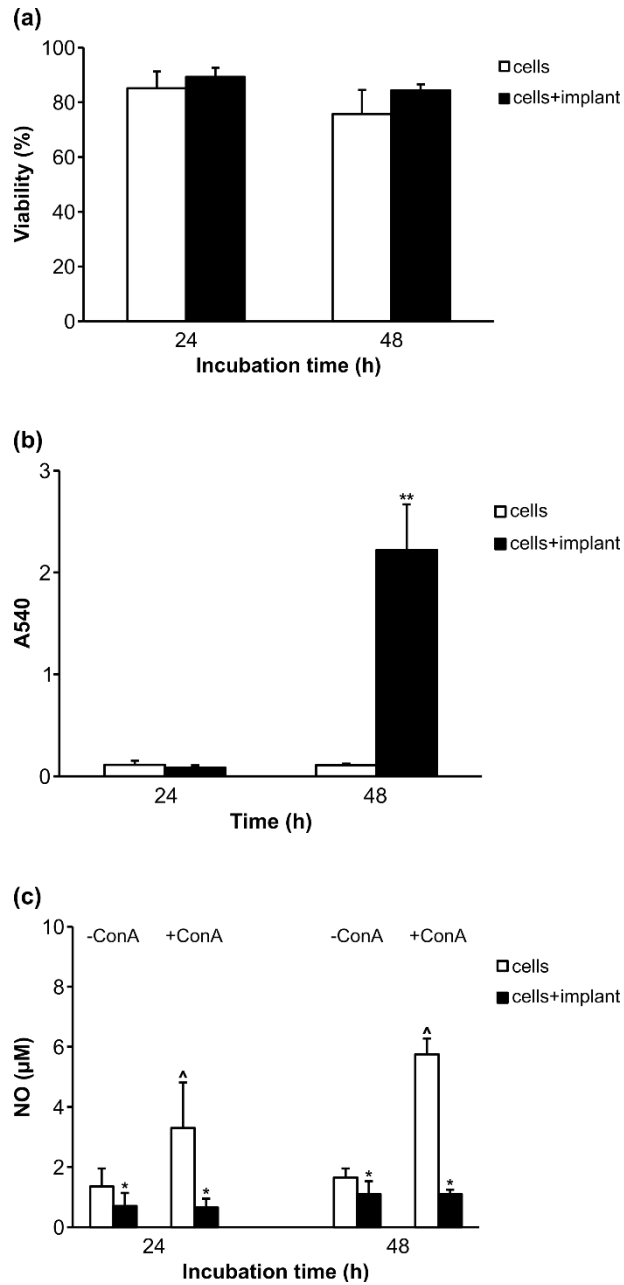
*Figure 5.* Metabolic activity and adhesion potential of L929 cells without (cells) and with (cells+implant) the implant: (a) MTT reduction and (b) Crystal violet test. Data are presented as the mean ± SD. Significance at: *$P < 0.05$ for cells vs cells+implant.

*Figure 6.* Viability, metabolic activity and NO production of spleen cells without (cells) and with (cells+implant) the implant: (a) Trypan blue exclusion, (b) MTT reduction, and (c) NO production. Data are presented as the mean ± SD. Significance at: *$P < 0.05$ and **$P < 0.01$ for cells vs cells+implant and ^$P < 0.05$ for non-stimulated (-ConA) vs ConA stimulated NO production (+ConA).
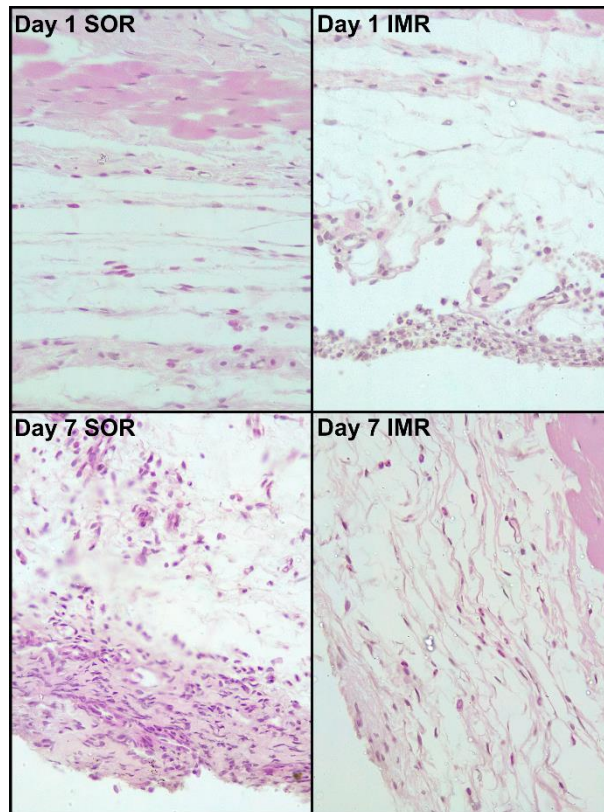
*Figure 7.* Representative skin histology (sham-operated rats (SOR), implanted rats (IMR), image magnification 40x). Day 1: Loose connective tissue in SOR and more compact connective tissue with clusters of cell debris in IMR. Day 7: Compact layer of connective tissue in SOR and a more edematous layer of connective tissue in IMR.
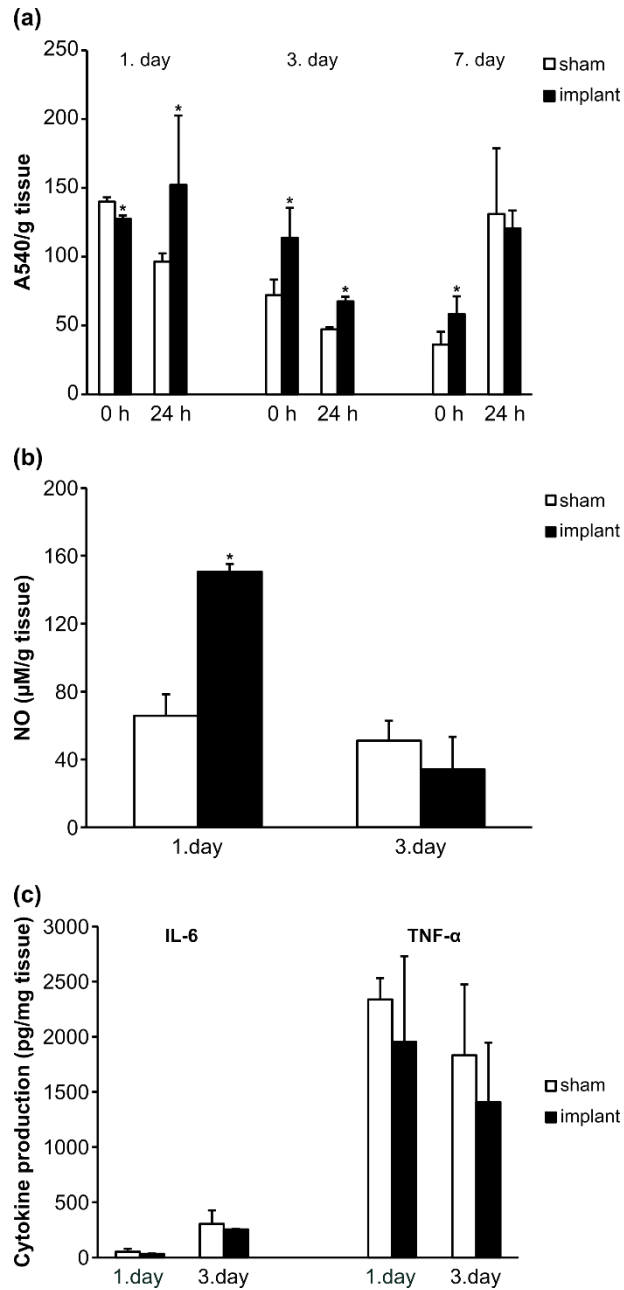
*Figure 8.* Local effects of implants on (a) MTT reduction, (b) NO production, and (c) cytokine production. Data are presented as the mean ± SD. Significance at: *$P < 0.05$ sham vs implant.
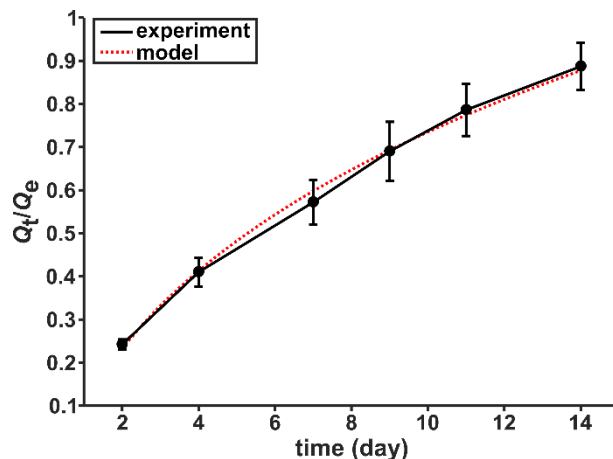
*Figure A1.* Comparison of the measured MB release kinetics from disk-shaped composite implants (solid line) and MB release kinetics predicted by the model for monolithic cylinders (dotted line). The parameter values are $D_a = 3.54 \times 10^{-13}$ m$^2$/s and $b = -0.2587$. Error bars shown for experimental points correspond to $\pm$ 3SD.
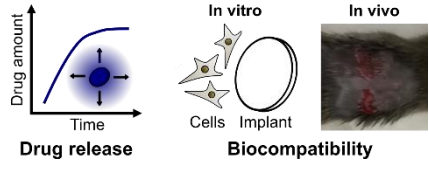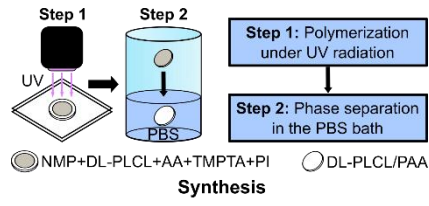
*Table 1.* Basic properties of prepared implants (MSD in PBS, WC, and Ccg) with their corresponding SDs

| Casting solution composition | MSD [%] | WC [%] | Ccg [mmol g$^{-1}$] |
|---|---|---|---|
| 16 wt% DL-PLCL | 346 ± 6 | 77.6 ± 0.3 | 2.06 ± 0.01 |
| 3.41 mmol g$^{-1}$ AA | | | |
| 10 mol% TMPTA | | | |

**Composite implantable reservoir for cationic drugs** is fabricated by a robust method combining photoirradiation and liquid phase inversion. Synthesized reservoir exhibits fast reversible swelling, excellent loading efficiency, good ion exchange capacity and diffusion-controlled release in vitro during two weeks. The unloaded reservoir has low acute toxicity and evokes a normal acute foreign body reaction in vivo.

Željko Janićijević, Marina Ninkov, Milena Kataranovski, Filip Radovanović*

**Poly(DL-lactide-*co*-ε-caprolactone)/poly(acrylic acid) composite implant for controlled delivery of cationic drugs**

**Step 1**
UV

**Step 2**
PBS

**Step 1**: Polymerization under UV radiation

**Step 2**: Phase separation in the PBS bath

NMP+DL-PLCL+AA+TMPTA+PI          DL-PLCL/PAA

**Synthesis**

Drug amount

Time

**Drug release**

**In vitro**

Cells    Implant

**In vivo**

**Biocompatibility**

# Supporting Information

**Poly(DL-lactide-*co*-ε-caprolactone)/poly(acrylic acid) composite implant for controlled delivery of cationic drugs**

Željko Janićijević, Marina Ninkov, Milena Kataranovski, Filip Radovanović*

# Supporting Information

## Poly(DL-lactide-*co*-ε-caprolactone)/poly(acrylic acid) composite implant for controlled delivery of cationic drugs

Željko Janićijević, Marina Ninkov, Milena Kataranovski, Filip Radovanović*

**MATLAB script: calculation of $D_a$ for cylindric composite reservoir geometry**

```
% Full model for monolithic cylinder diffusion with numerical approximation

% apparent diffusion coefficient D [m^2/s]
% measure of boundary layer resistance b
% FR = Mt/Minf = Qt/Qe is the fractional release

% Optimization with gradient descent method applied on b (flag = 1) and D (flag = 2)

clear all
clc
close all

% Implant geometry (cylinder dimensions measured by a caliper)
R = 6.5e-3; % cylinder radius [m]
H = 1.258e-3; % cylinder height [m]
L = H/2; % half of cylinder height (used in the model) [m]

% Measured values for the release kinetics of MB
t = 24*3600*[2,4,7,9,11,14,17,21,24,28]; % time points of MB release [s]
FR_m = [0.242,0.41,0.572,0.69,0.786,0.887,0.971,0.996,1,1]; % measured FR of MB
FR_m_std = [0.003961881,0.011236789,0.017368022,0.02284146,0.020116839,...
    0.018314712,0.007553963,0.001669337,3.24056e-05,0];% standard deviation
% of 3 experiments with FR measurements for MB

N = 6; % number of initial time points used for fitting
t_f = t(1:N); % time vector for fitting
FR_m_f = FR_m(1:N); % FR vector for fitting
FR_m_std_f =FR_m_std(1:N); % FR standard deviation for fitted points
FR_terms = zeros(N,4); % numerical approximation terms used in the model

% Initial values of variable parameters and steps for change
b = 0; % initial value of intercept corresponding to the boundary layer resistance
bs = 1e-4; % iterative step for b
step_sign_b = 1; % direction of change for b
D = 2.815e-13; % initial value of the apparent diffusion coefficient [m^2/s]
Ds = 1e-17; % iterative step for D
step_sign_D = 1; % direction of change for D

I = 0; % number of iterations
Imax = 2.5e4; % maximum number of iterations
FR_s = zeros(1,N); % simulated FR obtained by the model
SSE = zeros(1,Imax); % sum of squared errors
test = 1; % control parameter

% Implementation of the gradient descent algorithm

while test
```

```
    I = I + 1;

    % Calculation of the simulated FR at all time points
    for n = 1:N
        FR_terms(n,1) = ((D*t_f(n)/(L^2))^0.5)*(2/sqrt(pi) + 4*L/(R*sqrt(pi)));
        FR_terms(n,2) = -(D*t_f(n)/(L^2))*(8*L/(R*pi) + (L/R)^2);
        FR_terms(n,3) = ((D*t_f(n)/(L^2))^1.5)*((2/sqrt(pi))*(L/R)^2 - 1/(6*sqrt(pi))*(L/R)^3);
        FR_terms(n,4) = ((D*t_f(n)/(L^2))^2)*((1/(3*pi))*(L/R)^3 - (1/8)*(L/R)^4);
        FR_s(n) = sum(FR_terms(n,:))+ b;
    end

    SSE(I) = sum((FR_s-FR_m_f).^2);

    if I > 1
        delta = SSE(I)-SSE(I-1);

        if (delta > 0) && (flag == 1)
            step_sign_b = -step_sign_b;
        elseif (delta > 0) && (flag == 2)
            step_sign_D = -step_sign_D;
        end
        if mod(I,2) == 0
            D = D + step_sign_D*Ds;
            flag = 2;
        else
            b = b + step_sign_b*bs;
            flag = 1;
        end
    end

    if (I >= Imax)
        test = 0;
    end

end

Text_D =['Apparent diffusion coefficient is D = ',num2str(D) ,' m^2/s'];
disp(Text_D)

Text_b =['Intercept corresponding to the boundary layer resistance is b = ',num2str(b)];
disp(Text_b)
```

**Convergence plot of the gradient descent algorithm in the MATLAB script**
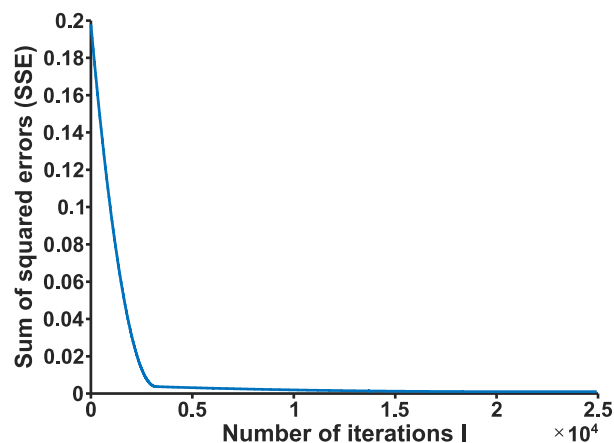


**Figure S1.** Convergence plot of the gradient descent optimization algorithm used to determine the apparent diffusion coefficient $D_a$ by fitting experimental data.

## Hematological parameters of rats

**Table S1**. Hematological parameters of sham-operated rats and rats with the implant.

| Parameter[a] | Day 1 Sham | Day 1 Implant | Day 3 Sham | Day 3 Implant | Day 7 Sham | Day 7 Implant |
|---|---|---|---|---|---|---|
| Le $10^9 L^{-1}$ | $8.4 \pm 2.7$[b] | $6.7 \pm 0.9$ | $11.8 \pm 0.2$ | $7.8 \pm 0.6$ | $10.0 \pm 0.6$ | $10.9 \pm 0.8$ |
| Ne % | $52.6 \pm 34.6$ | $40.0 \pm 16.9$ | $52.5 \pm 28.9$ | $30.0 \pm 0.1$ | $32.0 \pm 5.7$ | $31.1 \pm 4.4$ |
| Ly % | $46.0 \pm 34.0$ | $57.5 \pm 16.3$ | $44.5 \pm 28.9$ | $57.1 \pm 21.1$ | $66.1 \pm 5.6$ | $66.6 \pm 4.8$ |
| Mo % | $0.6 \pm 0.3$ | $0.9 \pm 0.3$*[c] | $0.8 \pm 0.1$ | $0.9 \pm 0.2$ | $0.7 \pm 0.2$ | $0.4 \pm 0.1$* |
| Eo % | $0.35 \pm 0.20$ | $0.7 \pm 0.2$* | $1.6 \pm 0.1$ | $1.6 \pm 0.3$ | $0.4 \pm 0.1$ | $1.4 \pm 0.3$* |
| Ba % | $0.5 \pm 0.3$ | $0.7 \pm 0.1$* | $0.5 \pm 0.1$ | $0.4 \pm 0.1$ | $0.7 \pm 0.1$ | $0.50 \pm 0.01$ |
| | | | | | | |
| RBC* $10^{12}$ | $7.2 \pm 0.4$ | $7.0 \pm 0.7$ | $7.0 \pm 0.1$ | $6.7 \pm 0.2$ | $6.6 \pm 0.3$ | $6.9 \pm 0.4$ |
| Hg g $L^{-1}$ | $131.0 \pm 5.7$ | $131.5 \pm 13.4$ | $127.5 \pm 2.1$ | $123.5 \pm 2.1$ | $124.5 \pm 4.9$ | $129.5 \pm 3.5$ |
| HCT I $I^{-1}$ | $0.40 \pm 0.03$ | $0.40 \pm 0.05$ | $0.40 \pm 0.01$ | $0.40 \pm 0.01$ | $0.40 \pm 0.02$ | $0.40 \pm 0.01$ |
| MCV fL | $57.0 \pm 0.3$ | $58.9 \pm 2.8$ | $58.3 \pm 1.1$ | $62.8 \pm 3.9$ | $64.5 \pm 0.3$ | $62.6 \pm 3.5$ |
| MCH pg | $18.3 \pm 0.3$ | $18.8 \pm 0.1$ | $18.2 \pm 0.1$ | $18.5 \pm 0.3$ | $18.9 \pm 0.1$ | $18.7 \pm 0.4$ |
| | | | | | | |
| MCHC g $L^{-1}$ | $321.5 \pm 6.4$ | $321.0 \pm 14.1$ | $321.0 \pm 5.6$ | $295.0 \pm 14.1$ | $293.5 \pm 0.7$ | $299.0 \pm 9.9$ |
| PLT *$10^9$ | $789.0 \pm 93.3$ | $719.0 \pm 90.5$* | $631.5 \pm 109.6$ | $625.5 \pm 139.3$ | $645.5 \pm 82.7$ | $716.0 \pm 91.9$ |
| MPV fL | $8.20 \pm 0.07$ | $8.3 \pm 0.2$ | $7.7 \pm 0.2$ | $7.9 \pm 0.1$ | $9.8 \pm 0.6$ | $9.7 \pm 0.1$ |
| PDW % | $40.9 \pm 1.1$ | $40.3 \pm 4.3$ | $39.3 \pm 2.0$ | $38.6 \pm 3.6$ | $43.1 \pm 4.1$ | $39.0 \pm 0.6$ |
| PCT L $L^{-1}$ | $0.6 \pm 0.1$ | $0.6 \pm 0.1$ | $0.5 \pm 0.1$ | $0.5 \pm 0.1$ | $0.6 \pm 0.1$ | $0.7 \pm 0.1$ |
| MPC g $L^{-1}$ | $195.0 \pm 1.4$ | $192.5 \pm 4.9$ | $184.5 \pm 4.9$ | $184.0 \pm 1.4$ | $165.5 \pm 0.7$ | $165.0 \pm 1.4$ |
| | | | | | | |
| PCDW g $L^{-1}$ | $48.4 \pm 0.1$ | $45.1 \pm 4.0$ | $42.7 \pm 0.6$ | $45.3 \pm 1.4$ | $49.1 \pm 0.1$ | $48.1 \pm 0.9$ |

[a]Abbreviations: Le-Leukocytes, Ne-Neutrophils, Ly-Lymphocytes, Mo-Monocytes, Eo-Eosinophils, Ba-Basophils, RBC-Red Blood Cells, Hg-Hemoglobin, HCT-Hematocrit, MCV-Mean Corpuscular Volume, MCH-Mean Corpuscular Hemoglobin, MCHC-Mean Corpuscular Hemoglobin Concentration, PLT-Platelet Count, MPV-Mean Platelet Volume, PDW-Platelet Distribution Width, PCT-Plateletcrit, MPC-Mean Platelet Component, PCDW-Platelet Component Distribution Width.;[b]Data are presented as the mean ± SD.; [c]Significance at *$P < 0.05$ sham vs implant.

**Histology of the implant/tissue interface**



Day 1 | Day 7
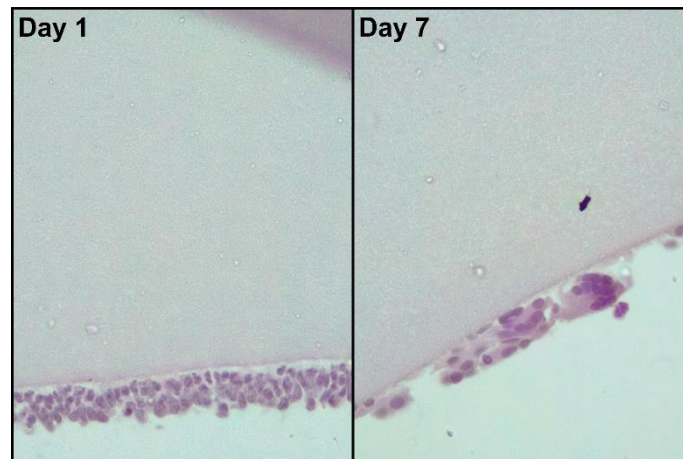
**Figure S2.** Implant/tissue interface at day 1 and day 7 (image magnification 63x). Cell infiltration is not observed.